

1 Effects of aquifer geometry on seawater intrusion in annulus
2 segment island aquifers

3
4 Zhaoyang Luo^{1,2}, Jun Kong^{1,3,#}, Chengji Shen¹, Pei Xin¹, Chunhui Lu¹, Ling Li⁴,
5 David Andrew Barry²

6
7 ¹State Key Laboratory of Hydrology-Water Resources and Hydraulic Engineering, Hohai
8 University, Nanjing, China

9
10 ²Ecological Engineering Laboratory (ECOL), Environmental Engineering Institute (IIE),
11 Faculty of Architecture, Civil and Environmental Engineering (ENAC), École Polytechnique
12 Fédérale de Lausanne (EPFL), Lausanne, Switzerland

13
14 ³Jiangsu Key Laboratory of Coast Ocean Resources Development and Environment Security,
15 Hohai University, Nanjing, China

16
17 ⁴School of Engineering, Westlake University, Hangzhou, China

18
19 #Corresponding author: Jun Kong (kongjun999@126.com)

20
21 Resubmitted to *Hydrology and Earth System Sciences*, on ~~27, August~~ 2021

Formatted: Indent: Left: 2 cm, Right: 2 cm

Deleted: 7

Formatted: Font: Not Bold, Not Italic

Deleted: 1

Deleted: February

25 **Abstract**

26 Seawater intrusion in island aquifers was considered analytically, specifically for annulus
27 segment aquifers (ASAs), i.e., aquifers that (in plan) have the shape of an annulus segment.
28 Based on the Ghijben-Herzberg and hillslope-storage Boussinesq equations, analytical
29 solutions were derived for steady-state seawater intrusion in ASAs, with a focus on the
30 freshwater-seawater interface and its corresponding watertable elevation. Predictions of the
31 analytical solutions compared well with experimental data, and so they were employed to
32 investigate the effects of aquifer geometry on seawater intrusion in island aquifers. Three
33 different ASA geometries were compared: convergent (smaller side facing the lagoon),
34 rectangular and divergent (larger side facing the sea). Depending on the aquifer geometry,
35 seawater intrusion was found to vary greatly, such that the assumption of a rectangular aquifer
36 to model an ASA can lead to poor estimates of seawater intrusion. Other factors being equal,
37 compared with rectangular aquifers, seawater intrusion is more extensive and watertable
38 elevation is lower in divergent aquifers, with the opposite tendency in convergent aquifers.
39 Sensitivity analysis further indicated that the effects of aquifer geometry on seawater intrusion
40 and watertable elevation vary with aquifer width and distance from the circle center to the
41 inner arc (the lagoon boundary for convergent aquifers while the internal no-flow boundary
42 for divergent aquifers). A larger aquifer width and distance from the circle center to the inner
43 arc, weaken the effects of aquifer geometry and hence differences in predictions for the three
44 geometries become less pronounced.

Formatted: Indent: First line: 2 ch, Line spacing: Double, No widow/orphan control

Formatted: Not Highlight

Formatted: Not Highlight

Formatted: Not Highlight

Formatted: Not Highlight

Formatted: Not Highlight

Deleted: to the (interior)

Deleted: no-flow boundary

Formatted: Font: 8 pt

Formatted: Font: 8 pt

47 **Keywords:** sharp-interface; steady-state analytical solution; atoll aquifer; annulus segment

48 aquifer, seawater intrusion,

Deleted: Page Break

49 **Key Points**

50 ➤ Analytical solutions of steady-state seawater intrusion were derived for annulus segment
51 aquifers

Deleted: a

52 ➤ Among three different aquifer geometries, divergent aquifers have the lowest watertable
53 and hence the most extensive seawater intrusion

54 ➤ Aquifer geometry effects on seawater intrusion depend on the aquifer width and distance
55 from the circle center to the inner arc

Formatted: Font: 8 pt

Formatted: Font: 8 pt

58 **1. Introduction**

59 Islands are extensively distributed ~~throughout the world's~~ oceans. ~~Unfortunately, their~~
60 ~~groundwater resources are impacted by~~ sea-level rise ~~and increased demands~~. According to a
61 recent estimate, there are approximately 65 million people living in oceanic islands where
62 ~~groundwater may be the only source of freshwater~~ (Thomas et al., 2020). Fresh groundwater
63 stored on oceanic islands is mainly ~~from precipitation~~ ~~(usually in the form of a freshwater~~
64 ~~lens)~~ and its availability ~~varies due to different~~ factors, ~~e.g.~~, island topography, rainfall
65 patterns, tides, episodic storms and human activities (White & Falkland, 2010; Storlazzi et al.,
66 2018). ~~Seawater intrusion is~~ ~~thus an~~ important issue ~~due to its deleterious effect on~~ oceanic
67 island freshwater storage (e.g., Werner et al., 2017; Lu et al., 2019; Memari et al., 2020).

68 ~~In contrast to~~ coastal aquifers where seawater intrudes into freshwater from one direction
69 only, seawater intrusion occurs from two directions for narrow strip islands and from all
70 directions for circular islands. Over the past few decades, seawater intrusion in oceanic
71 islands has been extensively investigated ~~in~~ field observations (e.g., Röper et al., 2013; Post et
72 al., 2019), ~~laboratory~~ experiments (e.g., Stoeckl et al., 2015; Bedekar et al., 2019; Memari et
73 al., 2020), numerical simulations (e.g., Lam, 1974; Gingerich et al., 2017; Liu & Tokunaga,
74 2019) and analytical solutions (e.g., Fetter, 1972; Ketabchi et al., 2014; Lu et al., 2019).

75 Among these, analytical solutions are effective tools to assess the extent of seawater intrusion
76 ~~(i.e., the location of the freshwater-seawater interface)~~, ~~although~~ they cannot incorporate
77 complex factors (e.g., dispersive mixing and transient oceanic dynamics) (Werner et al.,
78 2013). The advantages of analytical solutions are that ~~they are~~ ~~computationally efficient~~, ~~can~~

Deleted: in

Deleted: global

Deleted: and so are considered as vulnerable places due to

Deleted: and human population growth

Deleted: ,

Deleted: fresh

Deleted: recharged

Deleted: can be impacted by

Deleted:

Deleted: a variety of

Deleted: many

Deleted: including

Deleted: Among these, s

Deleted: another

Deleted: that greatly affects

Deleted: and is thus of considerable interest

Deleted: in multiple ways, either directly

Deleted: by

Deleted: or indirectly by

Deleted: al measurement

Deleted: ,

Deleted: despite that

Deleted: (1)

Deleted: rapidly and easily comput

Formatted: Font: 8 pt

Formatted: Font: 8 pt

103 ~~be used as test cases for numerical models, and can reveal the~~ explicit relationships between
104 parameters that influence seawater intrusion (e.g., Fetter, 1972; Ketabchi et al., 2014; Liu et
105 al., 2014; Lu et al., 2019).

Deleted: ed,

Deleted: (2) they

Deleted: give

Deleted: Liu et al., 2014

106 Based on the Dupuit-Forchheimer approximation (i.e., ignoring vertical flow) and ~~the~~
107 Ghijben-Herzberg equation (Drabbe & Badon Ghijben, 1889, English translation given by
108 Post (2018); Herzberg, 1901), Fetter (1972) presented analytical solutions describing the
109 freshwater-seawater interface location and watertable elevation in a circular island. Bailey et
110 al. (2010) further compared these single-layered analytical solutions with field measurements,
111 indicating that the analytical solutions perform well in estimating the freshwater-seawater

Deleted: the

112 interface location and watertable elevation. Fetter's solutions formed the ~~foundation~~ for many
113 ~~subsequent~~ analytical studies on seawater intrusion in island aquifers. ~~Again, for a single~~
114 ~~layer~~, Chesnaux and Allen (2008) and Greskowiak et al. (2013) developed analytical solutions
115 to predict the steady-state groundwater age distribution in freshwater lenses. In addition, using
116 ~~single-layered~~ analytical solutions, Morgan and Werner (2014) proposed vulnerability
117 indicators of freshwater lenses under sea-level rise and recharge change.

Deleted: (1972)

Deleted: funda

Deleted: ment

Deleted: that aimed at

Deleted: Based on this single-layered analytical theory

Deleted: the

118 Since aquifers are usually heterogeneous, the single-layer analytical solutions ~~were~~
119 ~~subsequently~~ extended to two-layered island aquifers, Vacher (1988) derived solutions for the
120 freshwater-seawater interface location and watertable elevation for infinite-strip islands
121 composed of different layers. Dose et al. (2014) ~~conducted~~ laboratory experiments to validate
122 ~~and confirm the reliability of~~ analytical solutions proposed by Fetter (1972) and Vacher
123 (1988). Ketabchi et al. (2014) extended Fetter's analytical solutions to calculate the

Deleted: in reality

Deleted: ed

Deleted: a

Deleted: subsequently

Deleted: arried out

Deleted: and confirmed their reliability

Deleted: (1972)

Formatted: Font: 8 pt

Formatted: Font: 8 pt

142 freshwater-seawater interface location and watertable elevation in two-layered circular islands
143 subject to sea-level rise. Their results indicated that land-surface inundation caused by sea-
144 level rise has a considerable impact on fresh groundwater lenses. Recently, Lu et al. (2019)
145 derived analytical solutions for the freshwater-seawater interface location and watertable
146 elevation for both strip and circular islands with two adjacent layers, i.e., a less permeable
147 slice along the shoreline of an island, and a more permeable zone inland.

148 All the abovementioned analytical solutions apply to either strip or circular islands.

149 According to the classification of sand dunes developed by Stuyfzand (1993; 2017), there are
150 different island layouts that should be considered, e.g., where the shape of the island is an
151 annulus segment, instead of a strip or circular disk (Figure 1). Annulus segment-shaped
152 islands are found in various atolls (i.e., circular chains of islands surrounding a central
153 lagoon) as found in the Pacific and Indian Oceans (Werner et al., 2017; Duvat, 2019).

154 Nevertheless, analytical solutions of seawater intrusion are not yet available for annulus
155 segment aquifers (ASAs). In general, ASAs are conceptually treated as a 2D cross section,
156 similar to strip islands (e.g., Ayers & Vacher, 1986; Underwood et al., 1992; Bailey et al.,
157 2009; Werner et al., 2017). Evidently, topography plays an important role in groundwater flow
158 and hence seawater intrusion (e.g., Zhang et al., 2016; Liu & Tokunaga, 2019). It remains
159 unclear whether analytical solutions of seawater intrusion for strip islands are appropriate for
160 ASAs. It is moreover additionally unclear how island geometry affects the freshwater-
161 seawater interface location and watertable elevation of ASAs.

162 In this study, analytical solutions are derived for steady-state seawater intrusion for ASAs,

Deleted: the

Deleted: . The analytical solutions of Ketabchi et al. (2014) and Vacher (1998) assumed an island with two horizontal layers...

Deleted: More r

Deleted: For more studies associated with regarding seawater intrusion in oceanic islands, readers are referred to the comprehensive review of Werner et al. (2017).

Deleted: Figure 1,

Deleted: le

Deleted: This configuration is

Deleted: widely distributed

Deleted: no

Deleted: have been

Deleted: developed

Deleted: like

Deleted: the

Deleted: s and

Deleted: we derive

Deleted: of the

Formatted: Font: 8 pt

Formatted: Font: 8 pt

183 with a focus on the freshwater-seawater interface location and its corresponding watertable
184 elevation. After comparing their predictions with experimental data (Memari et al., 2020), the
185 analytical solutions are employed to investigate the effects of aquifer geometry on the
186 freshwater-seawater interface location and watertable elevation in ASAs.

187 2. Conceptual Model

188 Figure 2 shows the conceptual model of an ASA (a slice of an atoll island). The plan
189 view of the model domain is represented as a sector ($EFGH$) with an angle θ (Figure 2a).
190 Radial flow only is considered. The sea (EF) and lagoon (HG) boundaries are located at L_+ and
191 L_0 [L] and L_0 [L] from the circle center, respectively. Since the longitudinal length is usually
192 much longer than the lateral length for an atoll island (Werner et al., 2017), seawater intrusion
193 from the lateral sides (EH and FG , Figure 2a) is negligible in comparison to the longitudinal
194 side, especially for the middle portion of an ASA. Therefore, EH and FG are treated as lateral
195 no-flow boundaries. Note that treating the lateral sides as no-flow boundaries is often used in
196 studies of freshwater lenses on atoll islands (e.g., Ayers & Vacher, 1986; Underwood et al.,
197 1992; Bailey et al., 2009; Werner et al., 2017). The side view of the model domain is
198 conceptualized as a rectangle ($ABCD$) along the radial direction with dimensions of L [L]
199 (width) \times d [L] (height) (Figure 2b,c). AD is the impermeable base while BC is the land
200 surface through which aquifer recharge flows.

201 Both the sea and lagoon water levels are set to H_s [L], which results in an internal no-
202 flow boundary (water divide, where the slope of the watertable is zero) between the sea and
203 lagoon (location of the z -axis in Figure 2b,c). The segment between the sea and the internal

Deleted: compiled from

Deleted: (

Deleted: s

Deleted: in reality

Deleted: it can be expected that

Deleted: would have

Deleted: influence on that from

Deleted: art

Deleted: In order t

Deleted: o facilitate analytical derivations, t

Deleted: It should be n

Deleted: d

Deleted: assuming

Deleted: boundary

Deleted: a

Deleted: y

Deleted: (e.g., EH and FG)

Deleted: has been

Deleted:

Deleted: widely adopted in previous

Deleted: related to

Deleted: and BC are

Deleted: and

Deleted: boundaries, respectively

Deleted:

Deleted: For simplicity, t

Formatted: Font: 8 pt

Formatted: Font: 8 pt

no-flow boundary is referred to as Unit 1, whereas the segment between the internal no-flow and lagoon boundaries is referred to as Unit 2 (Figure 2). The widths of Units 1 and 2 are l_1 [L] and l_2 [L], respectively. In addition, the flow is asymmetrical in Units 1 and 2, with divergent flow (the aquifer width w [L] increases along the flow direction) in Unit 1 and convergent flow (w decreases along the flow direction) in Unit 2.

The x - z coordinate origin is placed at the intersection of the internal no-flow boundary and impermeable base, with the x -axis pointing to the circle center and the z -axis pointing vertically upward. Further, ϕ [L] is the watertable height, h [L] is the vertical distance between the watertable and the interface, h_s [L] is the vertical distance between the sea level and the interface, and $h_c = H_s - h_s$ [L] is the vertical distance from the impermeable base to the interface for given x (Figure 2b,c). Constant recharge into the saturated zone, N [LT⁻¹], is assumed. There are two possibilities for the interface tip (i.e., the location where the freshwater-seawater interface connects to the z -axis or the bottom boundary): above the aquifer bed (Figure 2b) or on the aquifer bed (Figure 2c). The x -coordinates of the interface tip in Units 1 and 2 are denoted as x_{t1} [L] and x_{t2} [L], respectively (Figure 2c). Note that $x_{t1} = x_{t2} = 0$ when the interface tip is above the aquifer bed, as in Figure 2b.

Consistent with previous studies (e.g., Ketabchi et al., 2014; Lu et al., 2016; 2019), the following assumptions are made: (1) steady-state flow, (2) sharp freshwater-seawater interface, (3) homogeneous and isotropic aquifer, (4) negligible unsaturated flow, (5) recharge is less than the saturated hydraulic conductivity (else overland flow which will appear

- Deleted: ies
- Deleted: no-flow
- Deleted: length ...idth w [L] increases along the flow direction) in Unit 1 and convergent flow (the aquifer length ... [L]...
- Deleted: no-flow
- Deleted: horizontally
- Deleted: ... h [L] is the vertical distance between the watertable and the interface... h_s [L] is the vertical distance between the sea level and the interface, and $h_c = H_s - h_s$ [L] is the vertical distance from the impermeable base to the interface for given x (Figure 2b,c). Constant rR...charge into the saturated zone, N [LT⁻¹], is assumed to be uniform with value of N [LT⁻¹]
- Deleted: point...ocation where the freshwater-seawater interface connects to the no-flow boundary
- Formatted: Font color: Auto
- Deleted: location
- Deleted: and
- Formatted: Not Highlight
- Deleted: For the condition with the interface tip on the aquifer bed, t
- Formatted: Font: Italic
- Deleted: locations...(the location of the interface tip)
- Formatted
- Deleted: the...eady-state flow
- Deleted: system
- Deleted: is steady -state... (2) a
- Deleted: exists between freshwater and seawater
- Deleted: the...aquifer
- Deleted: hydraulic properties are
- Deleted: is homogeneous and isotropic... (4) negligible
- Deleted: ected
- Deleted: smaller ...ess than the saturated hydraulic
- Formatted

319 following ponding occurs), and (6) vertical flow in the saturated zone is negligible (Dupuit-
320 Forchheimer approximation).

321 3. Analytical Solutions

322 Groundwater flow in an ASA (Figure 2) can be described as (Paniconi et al., 2003; Troch
323 et al., 2003),

$$324 \quad -\frac{\partial}{\partial x}(wq) + Nw = \frac{\partial S}{\partial t} \quad (1)$$

325 where q [L^2T^{-1}] is the Darcy flux per unit length along the aquifer; S [L^2] is the total
326 water storage per unit distance along the aquifer, and t [T] is time. Equation (1) is derived
327 from the hillslope-storage Boussinesq equation reformulated in terms of soil water storage
328 rather than watertable elevation, as widely used previously (e.g., Stagnitti et al., 1986; Troch
329 et al., 2003; Hilberts et al., 2005; Kong et al., 2016; Luo et al., 2018). At steady state, equation
330 (1) reduces to,

$$331 \quad -\frac{\partial}{\partial x}(wq) + Nw = 0 \quad (2)$$

332 According to Darcy's law and the Dupuit-Forchheimer approximation, the freshwater
333 flux in the aquifer segment between the seaward boundary and interface tip can be calculated
334 as (ϕ is independent of z),

$$335 \quad q = -\int_{h_c}^{\phi} K_s \frac{d\phi}{dz} dz = -K_s (\phi - h_c) \frac{d\phi}{dx} \quad (3)$$

336 where K_s [LT^{-1}] is the saturated hydraulic conductivity.

337 3.1. Interface Tip above the Aquifer Bed

338 We first consider the situation where the interface tip is above the aquifer bed (Figure
339 2b). In Unit 1 where $w = \theta(L_0 + l_2 - x)$, substituting equation (3) into equation (2) and then

Deleted: will

Deleted:

Deleted: and analytical solutions cannot apply to

Deleted: no ponding

Deleted: is neglected

Deleted: ignorable

Deleted: i.e.,

Deleted: Derivation

Deleted:

Deleted: -

Deleted: can be

Deleted: d

Deleted: s

Formatted: Font: Italic

Field Code Changed

Formatted: Font: 8 pt

Formatted: Font: 8 pt

353 integrating gives (based on the Dupuit-Forchheimer approximation),

$$354 \quad -\frac{1}{2} \left[(L_0 + l_2 - x)^2 - (L_0 + l_2)^2 \right] N = -(L_0 + l_2 - x) K_s (\phi - h_c) \frac{d\phi}{dx} \quad (4)$$

355 According to the Ghijben-Herzberg equation, the vertical thickness of the freshwater zone (h)

356 in the interface zone is given by,

$$357 \quad h = \phi - h_c = (1 + \alpha)(\phi - H_s) \quad (5)$$

358 where $\alpha = \rho_f / (\rho_s - \rho_f)$ is the dimensionless density difference, and ρ_f [ML^{-3}] and ρ_s

359 [ML^{-3}] are the freshwater and seawater densities, respectively. Substitution of equation (5)

360 into equation (4) yields,

$$361 \quad -\frac{1}{2} \left[(L_0 + l_2 - x)^2 - (L_0 + l_2)^2 \right] N = -K_s (L_0 + l_2 - x) (1 + \alpha) (\phi - H_s) \frac{d\phi}{dx} \quad (6)$$

362 Rearranging equation (6) produces,

$$363 \quad -\frac{(L_0 + l_2 - x) N}{2} + \frac{N(L_0 + l_2)^2}{2(L_0 + l_2 - x)} = -K_s (1 + \alpha) (\phi - H_s) \frac{d\phi}{dx} \quad (7)$$

364 Integrating equation (7) leads to,

$$365 \quad -\frac{(L_0 + l_2)^2 N}{2} \ln(L_0 + l_2 - x) - \frac{1}{2} (L_0 + l_2) N x + \frac{1}{4} N x^2 + C_1 = -K_s (1 + \alpha) \frac{(\phi - H_s)^2}{2} \quad (8)$$

366 where C_1 is the integration constant that is determined by the sea boundary condition (i.e.,

367 $x = -l_1, \phi = H_s$),

$$368 \quad C_1 = \frac{(L_0 + l_2)^2 N}{2} \ln(L_0 + l_2 + l_1) - \frac{1}{2} (L_0 + l_2) l_1 N - \frac{1}{4} l_1^2 N \quad (9)$$

369 The relation between h_s and ϕ is given by,

$$370 \quad h_s = \alpha(\phi - H_s) \quad (10)$$

371 Combining equation (8) with equation (10) and eliminating ϕ yields,

Field Code Changed

Field Code Changed

Deleted: being

Deleted: densities of

Deleted:

Deleted: and can be

Formatted: Font: 8 pt

Formatted: Font: 8 pt

376
$$-\frac{(L_0+l_2)^2 N}{2} \ln(L_0+l_2-x) - \frac{1}{2}(L_0+l_2)Nx + \frac{1}{4}Nx^2 + C_1 = -K_s(1+\alpha)\frac{h_s^2}{2\alpha^2} \quad (11)$$

377 Equation (11) gives the freshwater-seawater interface location in Unit 1 once l_1 and l_2 are
378 determined.

379 Equation (8) applies to Unit 2 by replacing C_1 with C_2 ,

380
$$-\frac{(L_0+l_2)^2 N}{2} \ln(L_0+l_2-x) - \frac{1}{2}(L_0+l_2)Nx + \frac{1}{4}Nx^2 + C_2 = -K_s(1+\alpha)\frac{(\phi-H_s)^2}{2} \quad (12)$$

381 where C_2 is chosen to satisfy the lagoon boundary condition ($x=l_2$, $\phi=H_s$),

382
$$C_2 = \frac{(L_0+l_2)^2 N}{2} \ln(L_0) + \frac{1}{2}(L_0+l_2)l_2N - \frac{1}{4}l_2^2N \quad (13)$$

383 Combining equations (10) and (12) and eliminating ϕ generates,

384
$$-\frac{(L_0+l_2)^2 N}{2} \ln(L_0+l_2-x) - \frac{1}{2}(L_0+l_2)Nx + \frac{1}{4}Nx^2 + C_2 = -K_s(1+\alpha)\frac{h_s^2}{2\alpha^2} \quad (14)$$

385 Equation (14) gives the freshwater-seawater interface location in Unit 2 once l_2 is

386 determined. Since the sea level and lagoon water level are the same, an internal no-flow
387 boundary exists between the sea and lagoon, i.e.,

388
$$x=0, (h_s)_{unit1} = (h_s)_{unit2} \quad (15)$$

389 where $(h_s)_{unit1}$ and $(h_s)_{unit2}$ represent h_s in Units 1 and 2, respectively.

390 Combining equations (11), (14) and (15) leads to expressions for l_1 and l_2 ,

391
$$l_1 = L + L_0 - \sqrt{\frac{2LL_0 + L^2}{2\ln(L+L_0) - 2\ln(L_0)}} \quad (16)$$

392
$$l_2 = \sqrt{\frac{2LL_0 + L^2}{2\ln(L+L_0) - 2\ln(L_0)}} - L_0 \quad (17)$$

393 As indicated by equations (16) and (17), the internal no-flow boundary between the sea and

Deleted: can also

Deleted: y

Deleted: As mentioned before, s

Deleted: assumed to be

Deleted: no-flow

Field Code Changed

Field Code Changed

Formatted: Font: 8 pt

Formatted: Font: 8 pt

lagoon only depends on L and L_0 . For known l_1 and l_2 , equations (11) and (14) can be employed to predict the freshwater-seawater interface location in Units 1 and 2, respectively.

Once the interface location is determined, h and ϕ are given by,

$$h = \frac{1+\alpha}{\alpha} h_s \quad (18)$$

$$\phi = \frac{h_s}{\alpha} + H_s \quad (19)$$

3.2. Interface Tip on the Aquifer Bed

When the interface tip is on the aquifer bed, the location of the internal no-flow boundary remains the same as for the interface tip above the aquifer bed. The freshwater-seawater interface for Units 1 and 2 can be determined by equations (11) and (14),

respectively. Then, from equation (18), h at the aquifer segment between the sea boundary and the interface tip is determined. To calculate h for the aquifer segment between the interface tip and the internal no-flow boundary, the x -coordinate of the interface tip is found. At the interface tip of Unit 1 ($x = x_{i1}$),

$$h_s = H_s \quad (20)$$

$$\phi = \frac{1+\alpha}{\alpha} H_s \quad (21)$$

With equations (11) and (21), x_{i1} is given by,

$$-\frac{(L_0+l_2)^2 N}{2} \ln(L_0+l_2-x_{i1}) - \frac{1}{2}(L_0+l_2)Nx_{i1} + \frac{1}{4}Nx_{i1}^2 = -C_1 - K_s(1+\alpha)\frac{H_s^2}{2\alpha^2} \quad (22)$$

Let,

$$a = \frac{1}{4}N \quad (23a)$$

$$b = -\frac{1}{2}(L_0+l_2)N \quad (23b)$$

Deleted: under steady state

Deleted: we can further calculate

Deleted: as follows

Formatted: Font: 7 pt

Deleted: no-flow

Deleted: respectively

Deleted: we can calculate

Deleted: according to equation (18)

Deleted: .

Deleted: In order

Deleted: t

Deleted: calculate

Deleted: no-flow

Formatted: Font: Italic

Deleted: interface tip location

Deleted: should be determined first

Deleted:

Moved down [1]: ($x = x_{i1}$)

Moved (insertion) [1]

Deleted: we have,

Formatted: Font: 8 pt

Formatted: Font: 8 pt

436
$$c = -\frac{(L_0 + l_2)^2 N}{2} \quad (23c)$$

437 and

438
$$m = -C_1 - K_s(1 + \alpha)\frac{H_s^2}{2\alpha^2} \quad (23d)$$

439 then equation (22) becomes,

440
$$ax_{r1}^2 + bx_{r1} + c \ln(L_0 + l_2 - x_{r1}) = m \quad (24)$$

441 which is solved by a root-finding method.

442 The freshwater discharge for the aquifer segment between the interface tip and the

443 internal no-flow boundary is calculated as,

444
$$-\frac{1}{2} \left[(L_0 + l_2 - x)^2 - (L_0 + l_2)^2 \right] N = -(L_0 + l_2 - x) K_s \phi \frac{d\phi}{dx} \quad (25)$$

445 Repeating the steps from equations (4) to (8) gives,

446
$$-\frac{(L_0 + l_2)^2 N}{2} \ln(L_0 + l_2 - x) - \frac{1}{2} (L_0 + l_2) Nx + \frac{1}{4} Nx^2 + C_3 = -\frac{K_s}{2} \phi^2 \quad (26)$$

447 where C_3 is determined by substituting equation (21) into equation (26). Then, equation (26)

448 can be adopted to calculate h for the segment between the interface tip and the internal no-

449 flow boundary where $h = \phi$.

450 Similarly, the x-coordinate of the interface tip in Unit 2 (x_{r2}) is obtained by substituting

451 equation (20) into equation (14). Then, the watertable (h) of the aquifer segment between the

452 interface tip and the internal no-flow boundary for Unit 2 is computed by repeating the steps

453 from equations (22) to (26).

Deleted: no-flow

Deleted: can be

Deleted: no-flow

Deleted: interface tip location

Deleted: of

Deleted:

Formatted: Font: Italic

Deleted: 21

Deleted: a

Deleted: the value of

Formatted: Font: Not Italic

Deleted: for

Deleted: no-flow

Formatted: Font: 8 pt

Formatted: Font: 8 pt

4. Results and Discussion

4.1. Validation of the Analytical Solutions

The analytical solutions were validated by comparing their predictions with experimental data compiled from Memari et al. (2020), who reported experiments carried out using a 15° radial tank. The tank contained three distinct chambers: internal no-flow boundary condition, porous medium and constant-head boundary condition (i.e., sea or lagoon). The internal no-flow and seaward boundaries were respectively located at 10 cm and 55.5 cm from the circle center, i.e., 45.5 cm from the internal no-flow boundary to the constant-head boundary along the radial direction. Note that the experimental tank only corresponds to Unit 1 of the radial aquifer with $l_1 = 45.5 \text{ cm}$ and $l_2 = 0$, so the analytical results were calculated using equations (11) and (24). The thicknesses of the porous medium and sea level were 28 and 25 cm, respectively. The sand used in experiments had a saturated hydraulic conductivity of $1.23 \times 10^{-2} \text{ m s}^{-1}$ and an effective porosity of 0.40. The measured saltwater and freshwater densities were respectively 1.015 and 0.999 g ml^{-1} , leading to $\alpha = 62$. Two different recharge events with constant N , 2.46×10^{-4} and $1.08 \times 10^{-4} \text{ m s}^{-1}$, were considered in the experiments.

Figure 3 shows the comparison between analytical and experimental results of the freshwater-seawater interface for different recharge events. In general, the analytical solution predicts the freshwater-seawater interface well for both recharge events, despite there being some differences between the analytical results and the measurements, particularly in the zone near the constant-head boundary ($x = -45 \text{ cm}$). These deviations are likely due to assumptions made in the analytical solution, i.e., (i) a sharp freshwater-seawater interface, (ii) ignoring the

Deleted: . Their

Deleted: were

Deleted: that can be considered as an ASA

Deleted: radial

Deleted: no-flow

Deleted: seaward

Deleted: no-flow

Deleted: no-flow

Deleted: seaward

Deleted:

Deleted: (L^*).

Deleted: L^*

Deleted: while

Formatted: Font: Not Italic

Deleted: s

Deleted: XXX

Deleted: cm

Deleted: /

Formatted: Font: 小四, Superscript

Deleted: /

Formatted: Font: 小四, Superscript

Deleted: m s^{-1}

Deleted: m/s

Deleted: m/s

Deleted:

Deleted: For clarity, e

Deleted: The experimental parameters are summarized in Table 1....

Deleted: performs well in predicting t

Deleted: that there are small

Deleted: sea

Formatted: Font: 8 pt

Formatted: Font: 8 pt

514 effect of freshwater discharge, and (iii) neglecting the vertical flow (the Dupuit-Forchheimer
515 approximation).

516 4.2. Effects of Aquifer Geometry on Seawater Intrusion

517 Previous studies showed that boundary conditions play a critical role in estimates of
518 seawater intrusion (Werner & Simmons, 2009; Lu et al., 2016). Therefore, the internal no-
519 flow boundary between the sea and lagoon was examined for various ASAs. As indicated by
520 equations (16) and (17), this internal no-flow boundary depends only on L and L_0 . The values
521 of l_1 and l_2 calculated respectively from equations (16) and (17) are shown in Figure 4 for
522 three typical values of L (500, 1000, and 2000 m) with L_0 varying from 10^2 to 10^6 m. In
523 general, the internal no-flow boundary deviates from the middle of the ASA. When L_0 is less
524 than 10^5 m, l_1 is larger than l_2 for the three different values of L , indicating an internal no-
525 flow boundary closer to the lagoon boundary. For example, taking $L = 2000$ m and $L_0 = 100$ m
526 leads to $l_1 = 1240$ m and $l_2 = 760$ m, with a deviation of 240 m (12% of 2000 m) from the
527 middle of the ASA. When L_0 exceeds 10^5 m, however, the location of the internal no-flow
528 boundary can be approximated as being at the middle of the ASA for all considered values of
529 L . This is in contrast to strip and circular aquifers where the internal no-flow boundary is
530 always in the middle of aquifers due to symmetry.

531 Since the internal no-flow boundary location between the sea and lagoon deviates from
532 the middle of the ASA, we expect aquifer geometry to play a significant role in controlling
533 seawater intrusion. As mentioned previously, ASAs can be convergent (Unit 1) or divergent
534 aquifers (Unit 2) where the extent of seawater intrusion may be different. However, for strip

Deleted: indicated

Deleted: affecting

Deleted: no-flow

Deleted: (Table 1)

Deleted: no-flow

Deleted: only

Deleted: m

Deleted: m,

Deleted: varying

Deleted: no-flow

Deleted: smaller

Deleted: no-flow

Deleted: assuming

Deleted: no-flow

Deleted: to be

Deleted: no-flow

Deleted: ic flow

Deleted: Moreover, l_1 approaches l_2 with increasing L_0 , which suggests a movement of the no-flow boundary to the middle of the ASA. This is because, as L_0 increases, the island shape approaches to be increasingly approximates a rectangle with ular and hence leading to the flow parallel with to EH and FG . By comparison, at a given L_0 smaller than 10^5 m, the no-flow boundary location deviates more from the middle of the ASA with increasing L .

Deleted: no-flow

Formatted: Font: 8 pt

Formatted: Font: 8 pt

561 aquifers, both Units 1 and 2 are rectangular with the same extent of seawater intrusion.
562 Therefore, three geometries were compared in this study: convergent, rectangular and
563 divergent (Figure 5). These geometries have been widely examined in hillslope hydrology
564 regrading to the effects of aquifer geometry on runoff generation (Troch et al., 2003; Kong et
565 al., 2016; Luo et al., 2018). To present the results more conveniently, we replaced the x - z
566 coordinate origin at the intersection of the constant-head boundary (sea or lagoon) and the
567 impermeable base, with the x -axis pointing horizontally to the internal no-flow boundary and
568 the z -axis vertically upward (Figure 5). In addition, the distance between the constant-head
569 boundary and the internal no-flow boundary (aquifer width) is denoted as L^* (Figure 5) while
570 the other parameters remain the same.

571 Following previous studies (e.g., Lu et al., 2016; 2019), different cases were selected to
572 show the effects of aquifer geometry on seawater intrusion (Cases 1 and 2 in Table 1).
573 According to Werner et al. (2017), the width of atoll islands generally varies from 100 to 1500
574 m along the radial direction. In order to focus on the effects of aquifer geometry on seawater
575 intrusion, the same L^* and L_0 were assumed for the three aquifers, with L^* and L_0 equal to
576 1000 and 200 m, respectively. Note that L_0 is the distance from the circle center to the lagoon
577 boundary for convergent aquifers, whereas it represents the distance from the circle center to
578 internal no-flow boundary for divergent aquifers hereafter. The sand characteristics were the
579 same as in the experiments of Memari et al. (2020). Two recharge events were considered
580 (Cases 1 and 2, Table 1). The freshwater-seawater interface was calculated using the
581 analytical solutions for the three different aquifers. Note that the Appendix presents analytical

Deleted: For the sake of simplicity,

Deleted: seawater

Deleted: horizontally

Deleted: no-flow

Deleted: no-flow

Deleted: redefined

Formatted: Font: Italic

Formatted: Superscript

Deleted: keep

Deleted: hypothesized

Deleted: design

Deleted: m

Deleted: we assumed

Deleted: A

Formatted: Font: 8 pt

Formatted: Font: 8 pt

solutions for seawater intrusion in strip aquifers deduced from Lu et al. (2019).

Figure 6 shows the freshwater-seawater interface calculated for Cases 1 and 2. As can be seen, the extent of seawater intrusion is noticeably different for the three aquifer geometries. For high recharge ($1 \times 10^{-6} \text{ m s}^{-1}$), the interface tip is located at around 500 m for the divergent aquifer, which is about twice the value of the rectangular aquifer and six times the value for the convergent aquifer (Figure 6a). When the recharge decreases to $3 \times 10^{-7} \text{ m s}^{-1}$, the interface tip moves further landward for the three aquifers as expected, but the difference between results is still great (Figure 6b). The interface tip is displaced above the aquifer bed for both the rectangular and divergent aquifers, while it remains on the aquifer bed for the convergent aquifer. Regardless of the recharge rate, the most landward freshwater-seawater interface occurs in the divergent aquifer and vice versa for convergent aquifer. This underlines that aquifer geometry plays a major role in controlling seawater intrusion and hence it is necessary to account for aquifer geometry in analyses of seawater intrusion.

4.3. Sensitivity Analysis

A sensitivity analysis was conducted to investigate to what extent aquifer geometry affects seawater intrusion. Since we focus on the effects of aquifer geometry on the locations of the freshwater-seawater interface and watertable, values of L_0 and L^* were varied, with other parameters kept constant. When conducting the sensitivity analysis of L_0 , L^* was fixed at 1000 m, which is a typical value for ASAs (Werner et al., 2017). Figure 7 shows the sensitivity of the locations of the freshwater-seawater interface and watertable to changes in L_0 (Case 3, Table 1). The freshwater-seawater interface and watertable elevation are

- Deleted: greatly
- Deleted: different
- Deleted: the
- Deleted: give the value
- Formatted: Superscript
- Deleted:
- Deleted: m/s
- Deleted: more
- Deleted: of three aquifers
- Deleted: rises
- Deleted: s
- Deleted: s
- Deleted: significant
- Deleted: the
- Deleted: effects of
- Deleted: effects
- Deleted: tical solutions
- Deleted: will
- Deleted: A sensitivity analysis was conducted to investigate at which the degree to which of curvature the deviation of seawater intrusion between three different aquifers becomes significant...
- Deleted: thewe focus
- Deleted: is
- Deleted: on the effects of aquifer geometry on seawater intrusion...
- Deleted: that
- Deleted: the
- Deleted: depth
- Deleted: elevation
- Deleted: As expected, t
- Formatted: Font: 8 pt
- Formatted: Font: 8 pt

645 independent of L_0 for rectangular aquifers (Appendix). However, the freshwater-seawater
646 interface and watertable elevation differ greatly when varying L_0 for both convergent and
647 divergent aquifers, highlighting that L_0 plays an important role in affecting seawater intrusion.

648 Specifically, as L_0 increases, the freshwater-seawater interface moves more landward (larger
649 x/L^* , Figure 7a) and its corresponding watertable elevation decreases (Figure 7c) for

650 convergent aquifers. In contrast, for divergent aquifers increasing L_0 moves the freshwater-
651 seawater interface more seaward (smaller x/L^* , Figure 7b) and its corresponding watertable
652 elevation increases (Figure 7d). For a given L_0 , divergent aquifers have the largest extent of
653 seawater intrusion and the lowest watertable elevation, and conversely for convergent aquifers
654 (Figure 7).

655 Regardless of the freshwater-seawater interface and watertable elevation, the deviation
656 between rectangular aquifers and divergent or convergent aquifers is significant when L_0 is
657 less than 2000 m (Figure 7). For example, the x -coordinate of the interface tip ($z = 0$) is 262 m
658 for the rectangular aquifer at $L_0 = 200$ m, whereas it is 78 (31% of that in the rectangular
659 aquifer) and 500 m (191% of that in the rectangular aquifer) for the convergent and divergent
660 aquifers, respectively. As L_0 increases, the deviation between the three aquifers decreases.

661 When $L_0 = 2000$ m, the x -coordinate of the interface tip is 262, 209 (80% of that in the
662 rectangular aquifer) and 318 m (121% of that in the rectangular aquifer) for the rectangular,
663 convergent and divergent aquifers, respectively. As L_0 increases to 6000 m, the freshwater-
664 seawater interface and watertable elevation of both convergent and divergent aquifers tend to
665 those of rectangular aquifers, i.e., geometry effects decrease with increasing L_0 . These results

Deleted: L

Deleted: This is contrary to

Deleted:

Deleted: where for

Deleted: moves

Deleted: with increasing L_0

Deleted: Consistent with the experimental results of Hilberts et al. (2005), the steady-state watertable elevation is lower in the divergent aquifer than in the convergent aquifer for the same rainfall.

Deleted: By comparison,

Deleted: ,

Deleted: regardless of the freshwater-seawater interface and watertable elevation,

Formatted: Font: Italic

Deleted: toe location

Formatted: Font: Italic

Deleted: m

Formatted: Font: Not Italic

Formatted: Font: Italic

Formatted: Subscript

Deleted: the interface toe location

Deleted: When $L_0 = 2000$ m, the interface toe location is 262, 209 (80% of that in the rectangular aquifer) and 318 m (121% of that in the rectangular aquifer), respectively.

Deleted: continues to

Formatted: Font: 8 pt

Formatted: Font: 8 pt

687 highlight the critical role played by the shape of aquifers. As a result, ignoring geometry
688 effects may lead to an inappropriate management strategy for groundwater resources in atoll
689 islands.

690 The sensitivity of the freshwater-seawater interface and watertable elevation to L^* was
691 investigated by varying L^* from 600 to 1600 m while fixing L_0 to 200 m (Case 4, Table 1). As
692 shown in Figure 8, contrary to the results for varying L_0 , in this case the freshwater-seawater
693 interface and watertable elevation in all three topographies are related to L^* . Again, the extent
694 of seawater intrusion is greatest in divergent aquifers and least in convergent aquifers for
695 given L^* . When L^* increases, the freshwater-seawater interface moves seaward and the
696 watertable elevation increases, regardless of aquifer geometry, i.e., the seawater intrusion
697 decreases (Figures 8a-c). This is because the total freshwater flux increases with increasing
698 L^* , leading to a higher hydraulic gradient and hence less seawater intrusion (Figures 8d-f).

699 Moreover, an increase in L^* reduces the differences in the seawater intrusion distance among
700 the three geometries, i.e., geometry effects on seawater intrusion are more significant at small
701 L^* . However, even at the maximum L^* considered (1600 m), the deviation between three
702 aquifers remains significant: The x -coordinate of the interface tip is about 148 m for the
703 rectangular aquifer, whereas it is about 32 (22% of that in the rectangular aquifer) and 278 m
704 (188% of that in the rectangular aquifer) for the convergent and divergent aquifers,
705 respectively. Both L_0 and L^* can greatly impact seawater intrusion estimates for divergent and
706 convergent aquifers, highlighting the necessity to include geometry effects in analytical
707 solutions of seawater intrusion.

Deleted: fresh

Deleted: further conducted with

Deleted: at

Deleted: in

Formatted: Font: Not Italic

Deleted: is

Deleted: more

Deleted: induces a smaller deviation of

Deleted: between

Deleted: given in this study

Deleted: remain

Deleted: i

Deleted: s

Deleted: t

Deleted:

Formatted: Font: Italic

Deleted: interface toe location

Deleted: to

Formatted: Font: 8 pt

Formatted: Font: 8 pt

724 **5. Conclusions**

725 Based on the Ghijben-Herzberg and hillslope-storage Boussinesq equations, we derived
726 analytical solutions of steady-state seawater intrusion for ASAs, with a focus on the
727 freshwater-seawater interface and its corresponding watertable elevation as affected by
728 recharge. After comparing with experimental data of Memari et al. (2020), the analytical
729 solutions were employed to examine the effects of aquifer geometry on seawater intrusion in
730 island aquifers. Three different shapes of island aquifer were compared: convergent,
731 rectangular and divergent. The results lead to the following conclusions:

732 (1) The presented analytical solutions perform well in predicting the experimental
733 freshwater-seawater interface, suggesting that these analytical solutions can predict seawater
734 intrusion reasonably in different aquifer geometries.

735 (2) Island geometry plays a significant role in affecting the freshwater-seawater interface
736 and watertable elevation. Other factors being equal, the extent of seawater intrusion is greatest
737 in divergent aquifers, and conversely least in convergent aquifers. In contrast, the watertable
738 elevation is lowest in divergent aquifers and highest in convergent aquifers.

739 (3) The effects of aquifer geometry on seawater intrusion are dependent on the aquifer
740 width and distance from the circle center to the internal no-flow boundary (Figures 7 and 8).
741 A larger aquifer width and distance from the circle center to the inner arc (the lagoon
742 boundary for convergent aquifers while the internal no-flow boundary for divergent aquifers)
743 weakens the role played by aquifer geometry and hence lead to a smaller deviation of the
744 extent of seawater intrusion between the three topographies.

Deleted: for both recharge events

Deleted: T

Deleted: the most serious

Deleted: while the lightest

Deleted: the

Deleted: while

Deleted: the

Deleted: f

Deleted: no-flow

Deleted: xx

Formatted: Not Highlight

Deleted: Both a

Deleted: or

Deleted: from the circle center to the interior no-flow boundary

Deleted: can

Formatted: Font: 8 pt

Formatted: Font: 8 pt

760 Real island aquifers are expected to exhibit more complexity than considered here, e.g.,
761 that will have more complex shapes and are subjected to transient flow conditions caused by
762 tides, waves and pumping (Mantoglou et al. 2003; Pool & Carrera., 2011; Werner et al.,
763 2013). In addition, since the experimental scale of Memari et al. (2020) is necessarily small,
764 future experiments and field data are needed to further validate and facilitate the analytical
765 solutions. Despite this, the new analytical solutions, validated against experiments, can be
766 used as a tool to rapidly estimate seawater intrusion in ASAs once known island geometry and
767 corresponding soil properties are given.

Deleted: with regards to their topographies and subjecting to

Deleted: and

Deleted: fast

Formatted: Font: 8 pt

Formatted: Font: 8 pt

771 **Appendix: Analytical Solutions for Rectangular Aquifers**

772 For rectangular aquifers, the seawater intrusion in Unit 1 is identical to that in Unit 2
773 because of symmetry. With the interface tip on the aquifer bed, analytical solutions for the
774 freshwater-seawater interface (h_s), watertable elevation (h), and x -coordinate of the interface
775 tip in Unit 2 (x_{i2}) can be respectively written as (Lu et al., 2019),

$$776 \quad h_s = \alpha \sqrt{\frac{N}{(1+\alpha)K_s} \left(\frac{L^2}{4} - x^2 \right)} \quad (A1)$$

$$777 \quad h = \begin{cases} \sqrt{\frac{N}{K_s} (x_{i2}^2 - x^2) + \left(\frac{H_s}{\alpha} + H_s \right)} & 0 \leq x \leq x_{i2} \\ \sqrt{\frac{N}{(1+\alpha)K_s} \left(\frac{L^2}{4} - x^2 \right) + H_s} & x_{i2} < x \leq \frac{L}{2} \end{cases} \quad (A2)$$

$$778 \quad x_{i2} = \sqrt{\frac{L^2}{4} - \frac{(1+\alpha)K_s}{N} \left(\frac{H_s^2}{\alpha^2} \right)} \quad (A3)$$

779 When the interface tip is above the aquifer bed, the analytical solution for the freshwater-
780 seawater interface location and watertable elevation in Unit 2 are the same as equations (A1)
781 and (A2), respectively.

Deleted: A

Deleted: s

Deleted: ical groundwater flow

Deleted: of

Formatted: Subscript

Formatted: Font: Italic

Deleted: location (x)

Field Code Changed

Formatted: Font: 8 pt

Formatted: Font: 8 pt

787 **Code/Data availability**

788 Experimental data used in this study are compiled from Memari et al. (2020).

789 **Author contribution**

790 All authors contributed to the design of the research. ZL carried out data collation,
791 developed the analytical solutions and prepared the manuscript with contributions from all
792 co-authors. All authors contributed to the interpretation of the results and provided feedback.

793 **Competing interests**

794 The authors declare that they have no conflicts of interest.

795 **Acknowledgments**

796 This research was supported by the National Key R&D Program of China
797 (2019YFC0409004) and the National Natural Science Foundation of China (51979095,
798 41807178). ZL acknowledges EPFL for financial support and JK acknowledges the Qing Lan
799 Project of Jiangsu Province (2020).

800 **References**

801 Ayers, J. F., & Vacher, H. L. (1986). Hydrogeology of an atoll island: A conceptual model
802 from detailed study of a Micronesian example. *Groundwater*, 24(2), 185-198.

803 <https://doi.org/10.1111/j.1745-6584.1986.tb00994.x>

804 Bailey, R. T., Jenson, J. W., & Olsen, A. E. (2010). Estimating the ground water resources of
805 atoll islands. *Water*, 2(1), 1-27. <https://doi.org/10.3390/w2010001>

806 Bailey, R. T., Jenson, J. W., & Olsen, A. E. (2009). Numerical modeling of atoll island
807 hydrogeology. *Groundwater*, 47(2), 184-196. <https://doi.org/10.1111/j.1745->

808 [6584.2008.00520.x](https://doi.org/10.1111/j.1745-6584.2008.00520.x)

809 Bedekar, V. S., Memari, S. S., & Clement, T. P. (2019). Investigation of transient freshwater
810 storage in island aquifers. *Journal of Contaminant Hydrology*, 221, 98-107.

811 <https://doi.org/10.1016/j.jconhyd.2019.02.004>

812 Chesnaux, R., & Allen, D. M. (2008). Groundwater travel times for unconfined island
813 aquifers bounded by freshwater or seawater. *Hydrogeology Journal*, 16(3), 437-445.

814 <https://doi.org/10.1007/s10040-007-0241-6>

815 Dose, E. J., Stoeckl, L., Houben, G. J., Vacher, H. L., Vassolo, S., Dietrich, J., &

816 Himmelsbach, T. (2014). Experiments and modeling of freshwater lenses in layered
817 aquifers: Steady state interface geometry. *Journal of Hydrology*, 509, 621-630.

818 <https://doi.org/10.1016/j.jhydrol.2013.10.010>

819 Drabbe J. & Badon Ghijben, W. (1889). *Nota in verband met de voorgenomen put boring*
820 *nabij Amsterdam*, [Tiidschrift van het Koninklijk Instituut van Ingenieurs](#), pp. 8-22,

Deleted: ,

Deleted: *** Tijdschr. Kon. Inst. Ing.,*** Don't abbreviate

Formatted: Font: 8 pt

Formatted: Font: 8 pt

824 Gravenhage, Netherlands.

825 Duvat, V. K. E. (2019). A global assessment of atoll island planform changes over the past
826 decades. *Wiley Interdisciplinary Reviews: Climate Change*, 10(1), e557.
827 <https://doi.org/10.1002/wcc.557>

828 Fetter, C. W. (1972). Position of the saline water interface beneath oceanic islands. *Water
829 Resources Research*, 8(5), 1307-1315. <https://doi.org/10.1029/WR008i005p01307>

830 Gingerich, S. B., Voss, C. I., & Johnson, A. G. (2017). Seawater-flooding events and impact
831 on freshwater lenses of low-lying islands: Controlling factors, basic management and
832 mitigation. *Journal of Hydrology*, 551, 676-688.
833 <https://doi.org/10.1016/j.jhydrol.2017.03.001>

834 Greskowiak, J., Röper, T., & Post, V. E. (2013). Closed-form approximations for two-
835 dimensional groundwater age patterns in a fresh water lens. *Groundwater*, 51(4), 629-
836 634. <https://doi.org/10.1111/j.1745-6584.2012.00996.x>

837 Herzberg, A. (1901). Die wasserversorgung einiger Nordseebäder. *Journal für
838 Gasbeleuchtung und Wasserversorgung*, 44, 815-819, 45, 842-844.

839 Hilberts, A. G. J., Troch, P. A., & Paniconi, C. (2005). Storage-dependent drainable porosity
840 for complex hillslopes. *Water Resources Research*, 41(6), [W06001](https://doi.org/10.1029/2004WR003725).
841 <https://doi.org/10.1029/2004WR003725>

842 Ketabchi, H., Mahmoodzadeh, D., Ataie-Ashtiani, B., Werner, A. D., & Simmons, C. T.
843 (2014). Sea-level rise impact on fresh groundwater lenses in two-layer small islands.
844 *Hydrological Processes*, 28(24), 5938-5953. <https://doi.org/10.1002/hyp.10059>

Deleted: -

Formatted: Font: 8 pt

Formatted: Font: 8 pt

846 Kong, J., Shen, C., Luo, Z., Hua, G., & Zhao, H. (2016). Improvement of the hillslope-storage
847 Boussinesq model by considering lateral flow in the unsaturated zone. *Water*
848 *Resources Research*, 52(4), 2965-2984. <https://doi.org/10.1002/2015WR018054>

849 Lam, R. K. (1974). Atoll permeability calculated from tidal diffusion. *Journal of Geophysical*
850 *Research*, 79(21), 3073-3081. <https://doi.org/10.1029/JC079i021p03073>

851 Liu, J., & Tokunaga, T. (2019). Future risks of tsunami-induced seawater intrusion into
852 unconfined coastal aquifers: Insights from numerical simulations at Nijijima Island,
853 Japan. *Water Resources Research*, 55(12), 10082-10104.

854 <https://doi.org/10.1029/2019WR025386>

855 [Liu, Y., X. Mao, J. Chen, and D. A. Barry. 2014. Influence of a coarse interlayer on seawater](#)
856 [intrusion and contaminant migration in coastal aquifers. *Hydrological Processes*, 28\(20\),](#)
857 [5162-5175. <https://dx.doi.org/10.1002/hyp.10002>](#)

858 Lu, C., Cao, H., Ma, J., Shi, W., Rathore, S. S., Wu, J., & Luo, J. (2019). A proof-of-concept
859 study of using a less permeable slice along the shoreline to increase fresh groundwater
860 storage of oceanic islands: Analytical and experimental validation. *Water Resources*
861 *Research*, 55(8), 6450-6463. <https://doi.org/10.1029/2018WR024529>

862 Lu, C., Xin, P., Kong, J., Li, L., & Luo, J. (2016). Analytical solutions of seawater intrusion in
863 sloping confined and unconfined coastal aquifers. *Water Resources Research*, 52(9),
864 6989-7004. <https://doi.org/10.1002/2016WR019101>

865 Luo, Z., Shen, C., Kong, J., Hua, G., Gao, X., Zhao, Z., Zhao, H., & Li, L. (2018). Effects of
866 unsaturated flow on hillslope recession characteristics. *Water Resources Research*,

Formatted: Font: 小四
Formatted: Font: 小四, Not Bold, Italic
Formatted: Font: 小四
Formatted: Font: 小四

Formatted: Font: 8 pt
Formatted: Font: 8 pt

867 54(3), 2037-2056. <https://doi.org/10.1002/2017WR022257>

868 Mantoglou, A. (2003). Pumping management of coastal aquifers using analytical models of
869 saltwater intrusion. *Water Resources Research*, 39(12), 1335.
870 <https://doi.org/10.1029/2002WR001891>

Formatted: Font: 小四, Italic

Formatted: Font: 小四, Italic

Formatted: Font: 小四, Italic

Formatted: Font: 小四, Italic

871 Memari, S. S., Bedekar, V. S., & Clement, T. P. (2020). Laboratory and numerical
872 investigation of saltwater intrusion processes in a circular island aquifer. *Water*
873 *Resources Research*, 56(2), e2019WR025325. <https://doi.org/10.1029/2019WR025325>

874 Morgan, L. K., & Werner, A. D. (2014). Seawater intrusion vulnerability indicators for
875 freshwater lenses in strip islands. *Journal of Hydrology*, 508, 322-327.

876 <https://doi.org/10.1016/j.jhydrol.2013.11.002>

877 Paniconi, C., Troch, P. A., Van Loon, E. E., & Hilberts, A. G. (2003). Hillslope-storage
878 Boussinesq model for subsurface flow and variable source areas along complex
879 hillslopes: 2. Intercomparison with a three-dimensional Richards equation model.
880 *Water Resources Research*, 39(11), 1317. <https://doi.org/10.1029/2002WR001730>

881 Pool, M., & Carrera, J. (2011). A correction factor to account for mixing in Ghyben-Herzberg
882 and critical pumping rate approximations of seawater intrusion in coastal aquifers.
883 *Water Resources Research*, 47(5), W05506. <https://doi.org/10.1029/2010WR010256>

Formatted: Font: 小四, Italic

Formatted: Font: 小四, Italic

884 Post, V. E. (2018). Annotated translation of “Nota in verband met de voorgenomen putboring
885 nabij Amsterdam [Note concerning the intended well drilling near Amsterdam]” by J.
886 Drabbe and W. Badon Ghijben (1889). *Hydrogeology Journal*, 26(6), 1771-1788.

887 <https://doi.org/10.1007/s10040-018-1797-z>

Formatted: Font: 8 pt

Formatted: Font: 8 pt

888 Post, V. E. A., Houben, G. J., Stoeckl, L., & Sültenfuß, J. (2019). Behaviour of tritium and
889 tritiogenic helium in freshwater lens groundwater systems: Insights from Langeoog
890 Island, Germany. *Geofluids*, Volume 2019, Article ID 1494326,
891 <https://doi.org/10.1155/2019/1494326>

Deleted: *** 1-16

Deleted: *** Fix this: Geofluids Volume 2019, Article ID 1494326 ***

892 Röper, T., Greskowiak, J., Freund, H., & Massmann, G. (2013). Freshwater lens formation
893 below juvenile dunes on a barrier island (Spiekeroog, Northwest Germany). *Estuarine,
894 Coastal and Shelf Science*, 121-122, 40-50. <https://doi.org/10.1016/j.ecss.2013.02.004>
895 Stagnitti, F., Parlange, M. B., Steenhuis, T. S., & Parlange, J.-Y. (1986). Drainage from a
896 uniform soil layer on a hillslope. *Water Resources Research*, 22(5), 631-634.
897 <https://doi.org/10.1029/WR022i005p00631>

898 Stoeckl, L., Houben, G. J., & Dose, E. J. (2015). Experiments and modeling of flow processes
899 in freshwater lenses in layered island aquifers: Analysis of age stratification, travel
900 times and interface propagation. *Journal of Hydrology*, 529, 159-168.
901 <https://doi.org/10.1016/j.jhydrol.2015.07.019>

902 Storlazzi, C. D., Gingerich, S. B., van Dongeren, A., Cheriton, O. M., Swarzenski, P. W.,
903 Quataert, E., Voss, C. I., Field, D. W., Annamalai, H., Piniak, G. A., & McCall, R.
904 (2018). Most atolls will be uninhabitable by the mid-21st century because of sea-level
905 rise exacerbating wave-driven flooding. *Science Advances*, 4(4), eaap9741.
906 <https://doi.org/10.1126/sciadv.aap9741>

907 Strack, O. D. L. (1976). A single-potential solution for regional interface problems in coastal
908 aquifers. *Water Resources Research*, 12(6), 1165-1174.

Formatted: Font: 8 pt

Formatted: Font: 8 pt

912 <https://doi.org/10.1029/WR012i006p01165>
913 Stuyfzand, P. J. (2017). Observations and analytical modeling of freshwater and rainwater
914 lenses in coastal dune systems. *Journal of Coastal Conservation*, 21(5), 577-593.

915 <https://doi.org/10.1007/s11852-016-0456-6>
916 Stuyfzand, P. J. (1993). *Hydrochemistry and hydrology of the coastal dune area of the Western*
917 *Netherlands*. Ph.D. Thesis. Vrije University, Amsterdam, KIWA, ISBN 90-74741-01-
918 0. <http://dare.ubvu.vu.nl/handle/1871/12716>

919 Thomas, A., Baptiste, A., Martyr-Koller, R., Pringle, P., & Rhiney, K. (2020). Climate change
920 and small island developing states. *Annual Review of Environment and Resources*,
921 45(1), 1-27. <https://doi.org/10.1146/annurev-environ-012320-083355>

922 Troch, P. A., Paniconi, C., & Emiel van Loon, E. (2003). Hillslope-storage Boussinesq model
923 for subsurface flow and variable source areas along complex hillslopes: 1.
924 Formulation and characteristic response. *Water Resources Research*, 39(11), 1316.
925 <https://doi.org/10.1029/2002WR001728>

926 Underwood, M. R., Peterson, F. L., & Voss, C. I. (1992). Groundwater lens dynamics of atoll
927 islands. *Water Resources Research*, 28(11), 2889-2902.
928 <https://doi.org/10.1029/92WR01723>

929 Vacher, H. L. 1988. Dupuit-Ghyben-Herzberg analysis of strip-island lenses. *Geological*
930 *Society of America Bulletin*, 100, 580-591. [https://doi.org/10.1130/0016-](https://doi.org/10.1130/0016-7606(1988)100<0580:DGHAOS>2.3.CO;2)
931 [7606\(1988\)100<0580:DGHAOS>2.3.CO;2](https://doi.org/10.1130/0016-7606(1988)100<0580:DGHAOS>2.3.CO;2)

932 Werner, A. D., Sharp, H. K., Galvis, S. C., Post, V. E., & Sinclair, P. (2017). Hydrogeology

Deleted: ***

Deleted: *** correct use of uppercase/lowercase? ***

Deleted: ** comma or full stop needed here ***

Deleted: *** Univ. ***

Deleted: ***

Deleted: published by

Formatted: Not Highlight

Deleted: , 366 p*** . *** Is the period needed here? ***

Deleted: -

945 and management of freshwater lenses on atoll islands: Review of current knowledge
946 and research needs. *Journal of Hydrology*, 551, 819-844.

947 <https://doi.org/10.1016/j.jhydrol.2017.02.047>

948 Werner, A. D., Bakker, M., Post, V. E., Vandenbohede, A., Lu, C., Ataie-Ashtiani, B.,
949 Simmons, C. T., & Barry, D. A. (2013). Seawater intrusion processes, investigation
950 and management: Recent advances and future challenges. *Advances in Water*
951 *Resources*, 51, 3-26. <https://doi.org/10.1016/j.advwatres.2012.03.004>

952 Werner, A. D., & Simmons, C. T. (2009). Impact of sea-level rise on sea water intrusion in
953 coastal aquifers. *Groundwater*, 47(2), 197-204. [https://doi.org/10.1111/j.1745-](https://doi.org/10.1111/j.1745-6584.2008.00535.x)
954 [6584.2008.00535.x](https://doi.org/10.1111/j.1745-6584.2008.00535.x)

955 White, I., & Falkland, T. (2010). Management of freshwater lenses on small Pacific islands.
956 *Hydrogeology Journal*, 18(1), 227-246. <https://doi.org/10.1007/s10040-009-0525-0>

957 Zhang, Y., Li, L., Ertler, D. V., Santos, I., & Lockington, D. (2016). Effects of alongshore
958 morphology on groundwater flow and solute transport in a nearshore aquifer. *Water*
959 *Resources Research*, 52(2), 990-1008. <https://doi.org/10.1002/2015WR017420>

Deleted: r

Deleted:

Formatted: Font: 8 pt

Formatted: Font: 8 pt

962

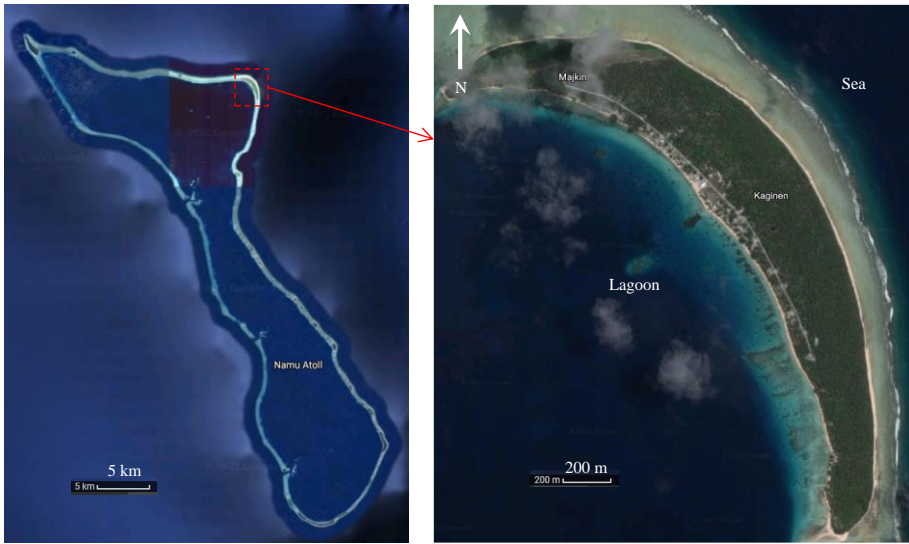
Table 1. List of parameters use in different simulations.

	<u>No.</u>	<u>L^* (m)</u>	<u>L_0 (m)</u>	<u>H_s (m)</u>	<u>d (m)</u>	<u>α (-)</u>	<u>n_e (-)</u>	<u>K_s (m s⁻¹)</u>	<u>N (m s⁻¹)</u>
	<u>1</u>	<u>1000</u>	<u>200</u>	<u>38</u>	<u>45</u>	<u>40</u>	<u>0.4</u>	<u>1.23×10^{-2}</u>	<u>1×10^{-6}</u>
<u>Cases</u>	<u>2</u>	<u>1000</u>	<u>200</u>	<u>38</u>	<u>45</u>	<u>40</u>	<u>0.4</u>	<u>1.23×10^{-2}</u>	<u>3×10^{-7}</u>
<u>Simulated</u>	<u>3</u>	<u>1000</u>	<u>‡</u>	<u>38</u>	<u>45</u>	<u>40</u>	<u>0.4</u>	<u>1.23×10^{-2}</u>	<u>1×10^{-6}</u>
	<u>4</u>	<u>‡</u>	<u>200</u>	<u>38</u>	<u>45</u>	<u>40</u>	<u>0.4</u>	<u>1.23×10^{-2}</u>	<u>1×10^{-6}</u>

963

‡The parameter is varied: The range of L_0 is from 200 to 6000 m, whereas the range of L^* is from 600 to 1600 m.

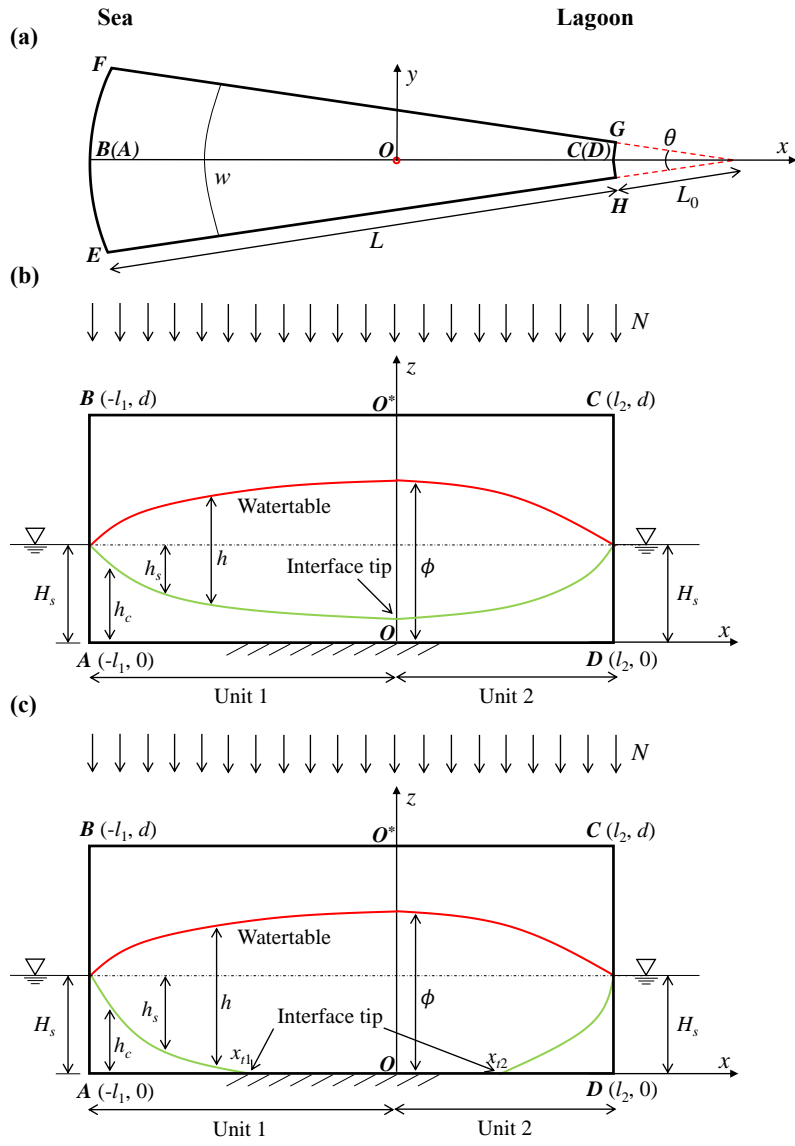
Deleted: .



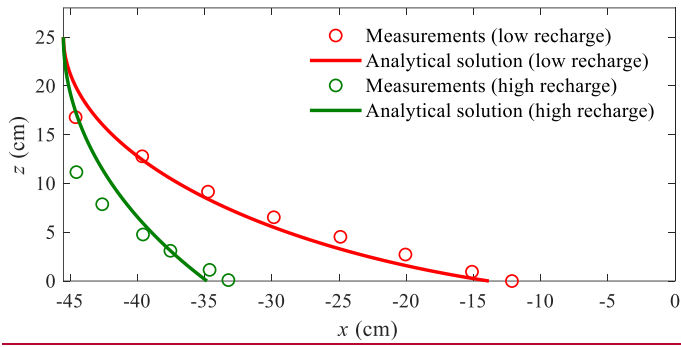
965

966 **Figure 1.** Island with an annulus segment in the Namu Atoll, Marshall Islands (© Google

967 Earth).



968
 969 **Figure 2.** Conceptual model of an annulus segment aquifer (a slice of an atoll island). (a) Plan
 970 view and (b, c) side view with the saltwater interface tip (b) above the aquifer bed (single
 971 location) and (c) on the aquifer bed (two locations). In (a), the sea boundary is on EF and the
 972 atoll lagoon boundary is on HG ; In (b) and (c), AD is the impermeable base and OO^* is the

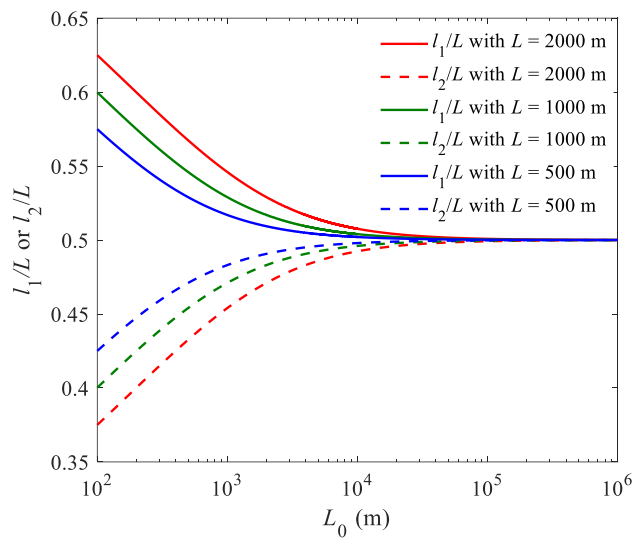


974

975 **Figure 3.** Comparison between analytical and experimental (data [compiled](#) from Memari et

976 al., 2020) results for the freshwater-seawater interface location for different recharge events.

977 Note that the left and right sides are the sea and [internal no-flow](#) boundaries, respectively. _____

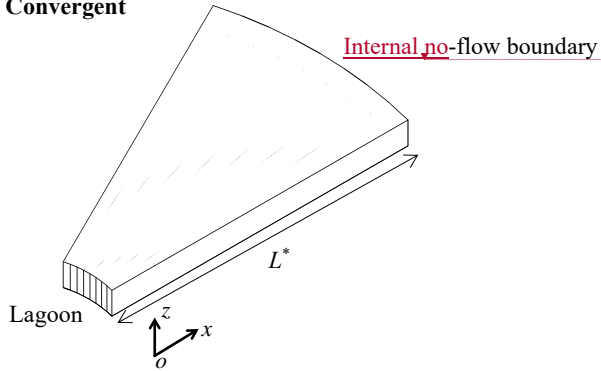


978

979

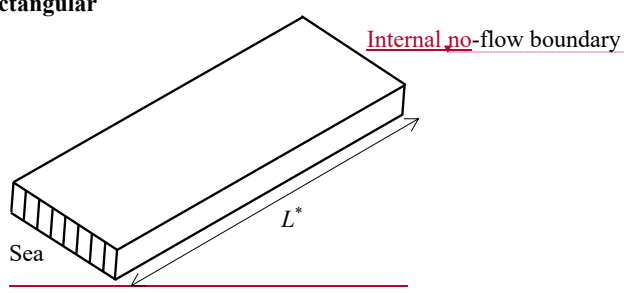
Figure 4. Widths of Unit 1 and Unit 2 versus L_0 for aquifers with different total width L .

(a) Convergent



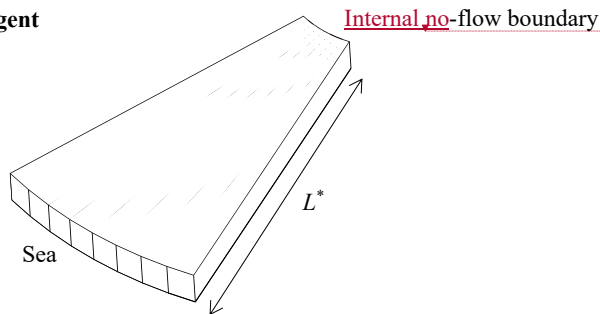
Deleted: No

(b) Rectangular



Deleted: No

(c) Divergent



Deleted: No

Figure 5. Three-dimensional view of (a) convergent (smaller side facing the lagoon), (b)

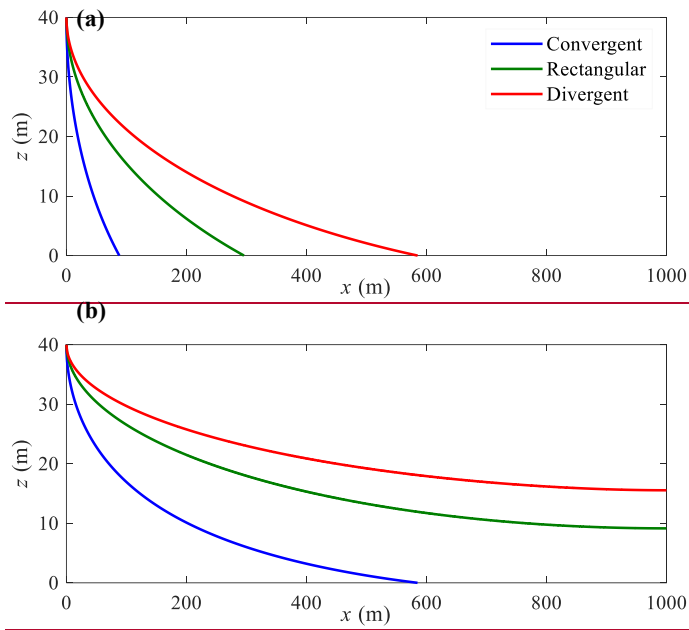
rectangular and (c) divergent aquifers (larger side facing the sea) compared in this study. L^*

represents the distance from the sea/lagoon to the internal no-flow boundary, i.e., l_1 or l_2 in

Field Code Changed

Field Code Changed

Figure 2. The internal no-flow boundary corresponds to the z-axis in Figure 2.



987

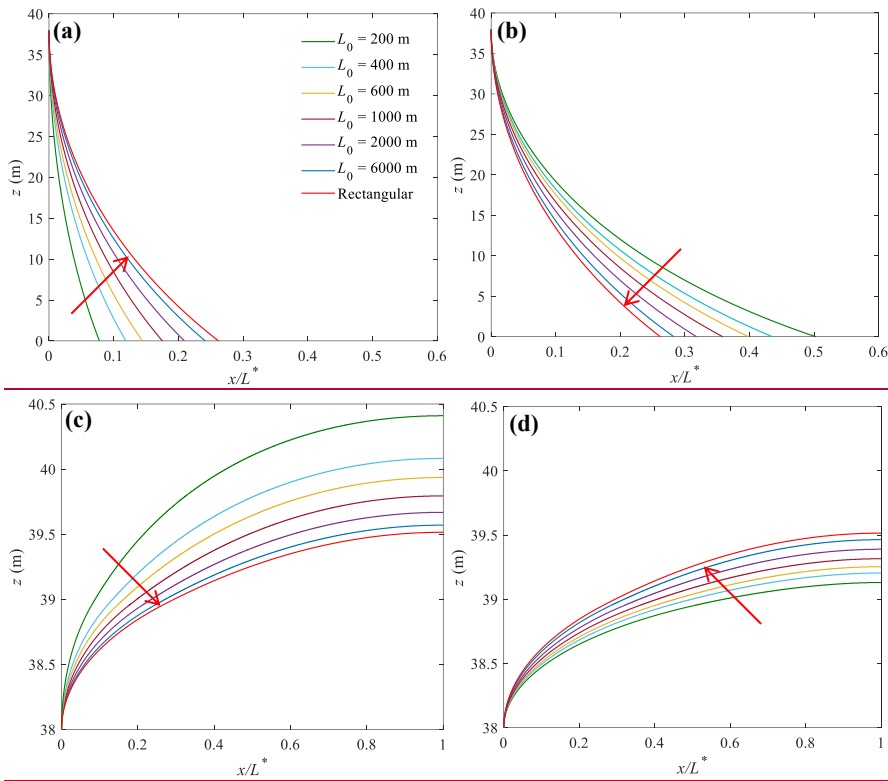
988

989

990

991

Figure 6. Freshwater-seawater interface predicted by analytical solutions for three different aquifers with (a) high and (b) low recharge (Cases 1 and 2 in Table 1). Note that $x = 1000$ m is the internal no-flow boundary in Figure 5.



992
993
994 **Figure 7.** Sensitivity of (a, b) the locations of the freshwater-seawater interface and (c, d)
995 watertable to L_0 for convergent (left panel) and divergent (right panel) aquifers. The arrow in
996 each plot shows the direction of increasing L_0 (values given in (a), used to produce the
997 different curves). Note that predictions for rectangular aquifers are independent of L_0 .

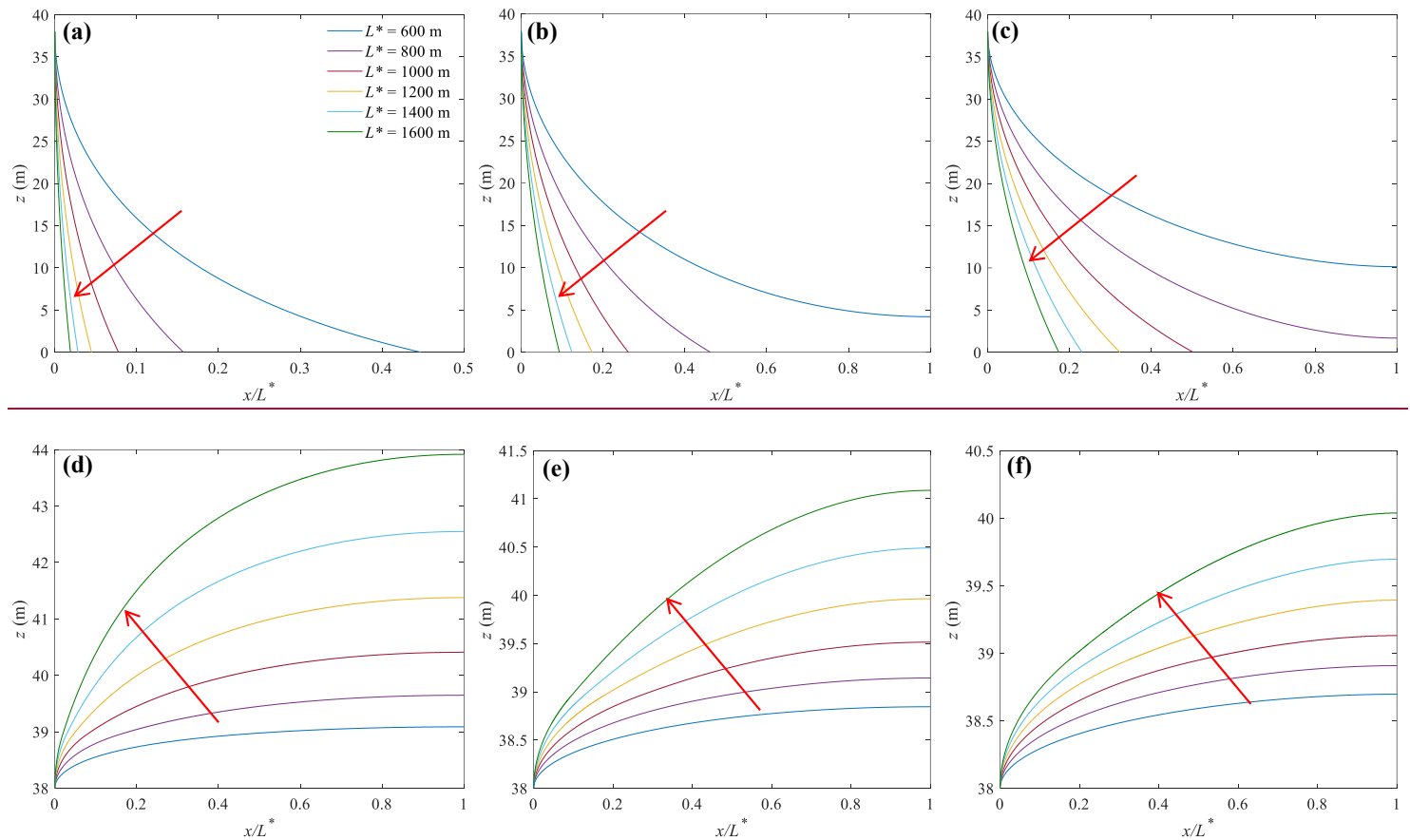


Figure 8. Sensitivity of (a-c) the locations of the freshwater-seawater interface and (d-f) watertable to L^* for convergent (a, d), rectangular (b, e)

- Formatted: Font: Not Bold
- Formatted: Font: Not Bold, Italic
- Formatted: Font: Not Bold, Superscript
- Formatted: Font: Not Bold
- Formatted: Font: 8 pt
- Formatted: Font: 10 pt

1001
1003

and divergent (c, f) aquifers. The arrow in each plot points to the increase of L_* values used to construct each curve (values indicated in (a)).

Formatted: Font: Not Bold, Italic

Formatted: Font: Not Bold, Superscript

Formatted: Font: Not Bold

Deleted: n plot

Formatted: Font: Not Bold

Formatted: Font: 8 pt

Formatted: Font: 10 pt